Interface Structure, Band Alignment, and Built-In Potentials at $LaFeO_3/n$-$SrTiO_3$ Heterojunctions

Ryan Comes[1,2] and Scott Chambers[1]
[1]Physical and Computational Sciences Directorate, Pacific Northwest National Laboratory, Richland, Washington 99352, USA
[2]Department of Physics, Auburn University, Auburn, Alabama 36849, USA
(Received 16 August 2016; published 22 November 2016)

Interface structure at polar-nonpolar interfaces has been shown to be a key factor in controlling emergent behavior in oxide heterostructures, including the $LaFeO_3/n$-$SrTiO_3$ system. We demonstrate via high-energy-resolution x-ray photoemission that epitaxial $LaFeO_3/n$-$SrTiO_3(001)$ heterojunctions engineered to have opposite interface polarities exhibit very similar band offsets and potential gradients within the $LaFeO_3$ films. However, differences in the potential gradient within the $SrTiO_3$ layer depending on polarity may promote hole diffusion into $LaFeO_3$ for applications in photocatalysis.

DOI: 10.1103/PhysRevLett.117.226802

Semiconducting perovskite oxides with the formula ABO_3, where B is a transition metal ion and A is a rare-earth or alkali-earth ion, are of growing interest for photocatalytic water splitting. Oxides are far more stable in the terrestrial atmosphere than are traditional semiconductors. Likewise, the prospects for stability in aqueous solutions are better for oxides, particularly near neutral pH. For good solar photocatalytic performance, a band gap of approximately $\sim$1.5 eV is ideal [1], making Fe-based oxides such as α-Fe_2O_3 [2] and $LaFeO_3$ [3,4] (LFO) attractive candidates. A 2.3 eV direct band gap has been reported for epitaxial thin films of LFO [5], while doping with Sr enhances light absorption at lower photon energies [6]. Effective spatial separation of optically excited electron-hole pairs is also desirable to enhance carrier lifetimes. One approach to solve this problem is the use of a ferroelectric oxide which has an intrinsic electric field to separate electrons and holes [7]. This approach has been used to good effect in $BiFeO_3$ epitaxial thin films with a band gap comparable to LFO [8].

Recent reports of interface-induced polarization for LFO films grown on Nb-doped $SrTiO_3$ (n-STO) have spurred interest in understanding electronic reconstruction at the junction of these perovskites [9,10]. M. Nakamura *et al.* [9] report that growing LFO on both SrO- and TiO_2-terminated n-STO(001) substrates results in polarization in the films but with the polarization dependent on the interface structure. SrO-terminated STO(001) was generated by preparing a TiO_2-terminated substrate using conventional wet chemical etching using HF acid [11] followed by the deposition of a single monolayer of SrO. For LFO films grown on SrO-terminated (TiO_2-terminated) STO, the idealized heterojunction would be negatively (positively) charged with an SrO^0-FeO_2^- ($TiO_2{}^0$-LaO^+) interface. These authors report zero-bias, visible-light photocurrents flowing in opposite directions depending on the interfacial termination. This result was attributed to bulk polarizations in the material, as previously predicted under extremely high strain ($\sim$9%) in rare-earth ferrites [12]. In the absence of high strain (the lattice mismatch between LFO and n-STO is only $\sim$1%), the authors posit that the induced polarization is driven by differing interface dipoles and polar discontinuities. Subsequently, independent work by K. Nakamura *et al.* [10] employed an identical experimental approach and also found that visible-light photoconductivity at zero bias was dependent on the interface structure. In the work of K. Nakamura [10], visible-light photocatalytic responses were also observed with minimal dependence on interfacial structure for $h\nu < 2.9$ eV. A much stronger response was observed for $h\nu > 3.2$ eV (i.e., above the band gap of STO) for specimens with the SrO-FeO_2 interface. This result was attributed to differing electronic reconstructions leading to either accumulation (TiO_2-LaO^+) or depletion (SrO-$FeO_2{}^-$) at the heterojunction. These intriguing results motivate additional experiments aimed at detecting the presence (or absence) of oppositely oriented built-in potentials and polarizations within LFO films.

To this end, we prepared a series of LFO/n-STO(001) heterojunctions using oxygen-assisted molecular beam epitaxy (MBE) and carried out interface electronic structure measurements using high-energy-resolution x-ray photoelectron spectroscopy (XPS) and spectroscopic ellipsometry (SE). All films were grown at $600 \pm 50\,^{\circ}$C at a rate of one LaO or FeO_2 monolayer every 43 s using effusion cells and alternately shuttering the La and Fe beams, with a mixed O/O_2 beam generated by an electron cyclotron resonance source continuously incident on the substrate [13]. A pair of 0.05% Nb-doped STO substrates (Crystec) were prepared side by side using a boiling deionized water treatment [14], followed by an anneal in air at $1000\,^{\circ}$C for 30 min. The samples were then cleaned in ozone on the bench and loaded into an oxide MBE system with an appended x-ray photoelectron spectrometer (VG Scienta

R3000 analyzer and monochromatic Al $K\alpha$ x-ray source). The TiO_2 surface termination was confirmed using angle-resolved XPS measurements [15]. A single monolayer of SrO was then deposited using an effusion cell on one of the substrates to achieve the *A*-site termination, also confirmed by angle-resolved XPS. After preparing the two substrates, increments of three unit cells (u.c., 1 u.c. = ~3.9 Å) of LFO were grown with a shuttering sequence configured to match the substrate termination [i.e., FeO_2 (LaO) layer deposited on the SrO (TiO_2) termination]. *In situ* reflection high-energy electron diffraction (RHEED) was used to monitor the surface structure during growth, as can be seen in Fig. S1 [15].

In situ XPS band alignment measurements were made following each 3 u.c. deposition, with a separate thick (~12 nm) LFO film grown to determine the bulk electronic structure of the material. Details of band alignment analysis are described elsewhere [13] and can be found in Supplemental Material [15]. In brief, the energy separation between core levels unique to the film and the substrate were used to extract the valence band offset (VBO), assuming that there is no differential charge accumulation between the film and substrate due to photoemission. We saw no evidence of charging for the 3, 6, and 9 u.c. films. However, the 12 nm LFO films did accumulate charge, and a low-energy electron flood gun was used to neutralize this charge. The energy scale was calibrated using a constant offset such that the O 1*s* singlet was at the same binding energy as that for the 9 u.c. *A*-site-terminated LFO film (529.2 eV).

Figure 1 summarizes the relevant spectra for all LFO/*n*-STO heterostructures, STO substrates, and thick LFO films. The Sr 3*d* and La 4*d* peaks in Fig. 1(a) have been shifted slightly so that all Sr $3d_{5/2}$ peaks are aligned at 0 eV as a means of visualizing the separation between the Sr 3*d* and La 4*d* peaks, which increases with increasing thickness. This monotonic shift reveals changes in the built-in potential and band alignment with thickness, as has been reported previously in $LaCrO_3$ films grown on STO [17,18] and in LFO films grown on arbitrarily terminated *n*-STO [19]. The

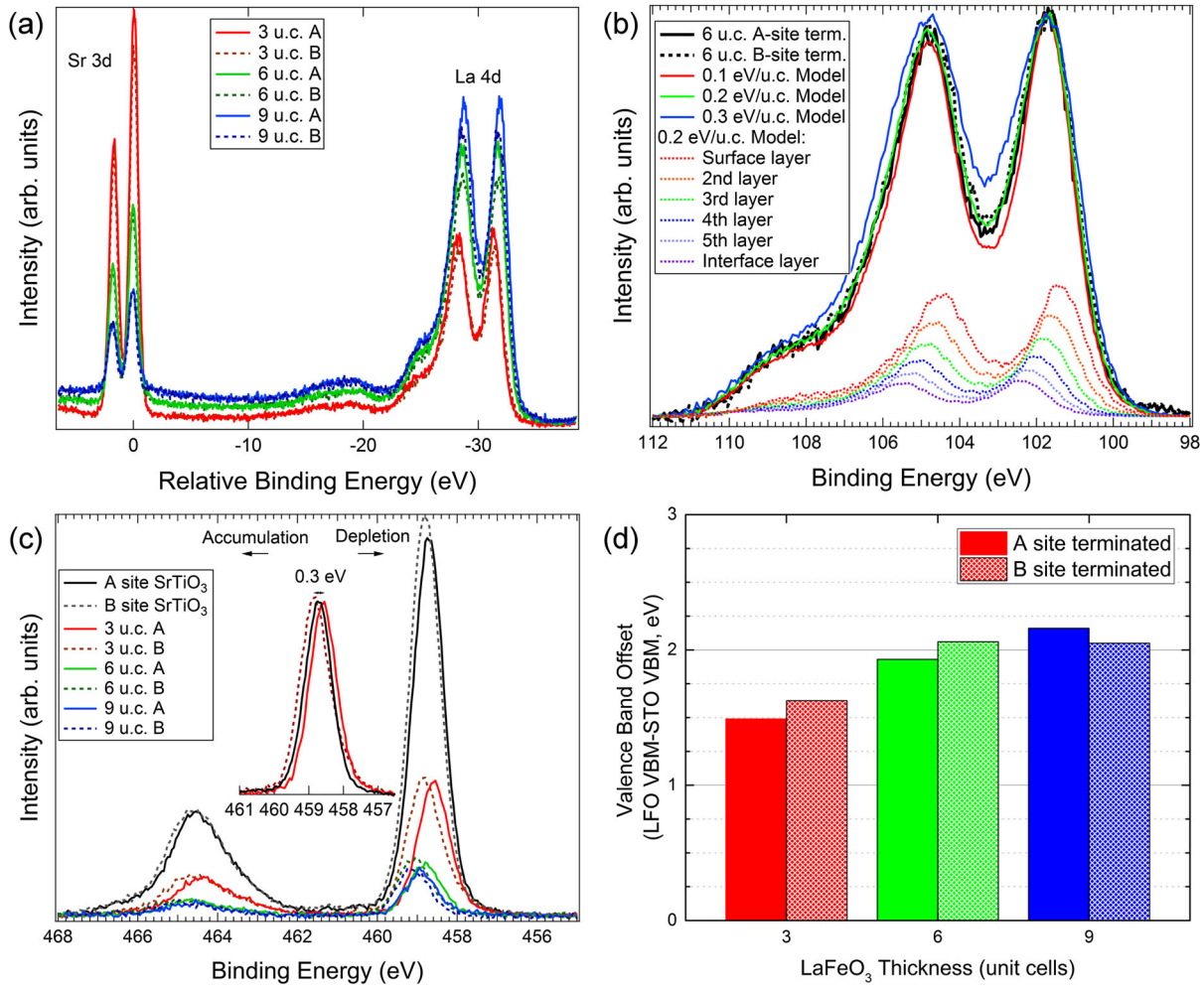

FIG. 1. (a) Sr 3*d* and La 4*d* core-level spectra for the family of heterostructures, shifted to align the Sr 3*d* peaks; (b) model of La 4*d* peak broadening in the 6 u.c. films; (c) Ti 2*p* core-level spectra for each film and substrate, with the inset showing the peak shifts; (d) valence band offsets determined from the core-level spectra for each heterojunction.

La 4d peaks for both A- and B-site-terminated films move to a lower binding energy with increasing thickness, indicating that the VBO increases with thickness and that the LFO valence band maximum (VBM) moves closer to the Fermi level (E_F). From these spectra, the VBOs are readily determined, as described below.

The La 4d core level peaks for the thin-film heterostructures are broader than those for the thick reference LFO films, which are nominally flat band. This result is consistent with the presence of a built-in potential within the thinner films. By modeling this broadening to account for contributions of each unit cell, we can estimate these potential gradients [15]. The broadening is nearly identical for both the A-site- and B-site-terminated samples for each thickness, revealing that the potential gradient within the LFO is the same for both interface terminations. This experimental result contradicts previous work in which potential gradients of opposite sign were assumed for the two terminations in order to explain photoconductivity data [9]. We measure built-in potentials of 0.3 eV/u.c. for the 3 u.c. film and 0.2 eV/u.c. for the 6 u.c. film for both interface polarities. This allows us to estimate the change in the electrostatic potential from the film surface to the film-substrate interface. The uncertainty in the potential in each layer is estimated by varying the potential at each unit cell in the stack until the fit to the data is clearly worse than the initial model. This produces uncertainties of 0.1 eV near the film surface and 0.2–0.3 eV deeper within the film. We see comparable broadening between the 6 and 9 u.c. thick films, but our analysis indicates that the 9 u.c. film has reached a flat-band condition after completion of 6 u.c.

Although there is no measurable dependence of the potential gradient within the LFO on interface structure, more subtle observations help to elucidate the nature of the interface. As can be seen in Fig. 1(c), the Ti 2p core-level binding energy and peak shape depend on the interfacial termination. The TiO_2-terminated heterojunctions exhibit uniformly higher binding energies than their SrO-terminated counterparts. Furthermore, the Ti $2p_{3/2}$ peak for the TiO_2-terminated 3 u.c. heterojunction exhibits an asymmetry to low binding energy, in contrast to the STO substrates and the SrO-terminated 3 u.c. interface, all of which are symmetric (see the inset). Similar behavior is seen in the 6 u.c. TiO_2-terminated case, but the strong attenuation from the thicker 9 u.c. film prevents rigorous analysis for the 9 u.c. sample. No broadening is observed for any SrO-terminated sample. The Ti $2p_{3/2}$ peak energy for the B-site-terminated interface is shifted 0.3 eV to higher binding energy compared to the A-site-terminated sample. This difference is consistent with the presence of a fixed positive (negative) charge at the TiO_2^0-LaO^+ (LaO^+-FeO_2^-) interface. Similar binding energy shifts are observed for the Sr 3d core level. The low binding energy shoulder seen in the Ti $2p_{3/2}$ spectra for the B-site-terminated specimens could result from outdiffused Ti within the first u.c. of LFO. The energy difference between this feature and the substrate Ti $2p_{3/2}$ peak is consistent with the valence band discontinuity when a correction is made for the width of the Fe 3d derived feature at the top of the LFO VB, as seen in Fig. 3(a) and described in Supplemental Material [15]. The B-terminated interface between STO and $LaAlO_3$ is also known to exhibit a greater amount of intermixing in previous work [20], in agreement with our conclusion.

The VBOs determined from fits of the Ti 2p, Sr 3d, La 4d, and Fe 3p spectra in Figs. 1(a)–1(c) are shown in Fig. 1(d). The uncertainties in these measurements are ± 0.1 eV in each case. We find that the interfacial termination has a negligible effect on the VBO, indicating that there is no divergence in the potential due to an induced ferroelectric-type polarization, in contrast to the behavior others have reported [9,10]. Instead, the VBO increases with increasing LFO thickness and saturates at 2.0–2.2 eV, close to the value previously reported for arbitrarily terminated n-STO [19].

To estimate the conduction band offset, SE measurements were performed to determine the band gap of LFO using a 12 nm thick film grown on undoped STO. The results of fits to the data are shown in Fig. 2. Various groups have used values of 2.0 [19], 2.1 [10], and 2.2 eV [9] in their analysis of the LFO/n-STO band alignment. However, computational and experimental studies by Scafetta *et al.* [5] have shown that the band gap is 2.3 eV when the optical transition is modeled as a direct-forbidden excitation from the hybridized majority-spin Fe 3d e_g and O 2p VB maximum to the unfilled minority-spin Fe 3d t_{2g} conduction band (CB) minimum. This method involves extrapolating the linear region of the quantity $(\alpha h\nu)^{2/3}$ to the energy axis. Here α is the

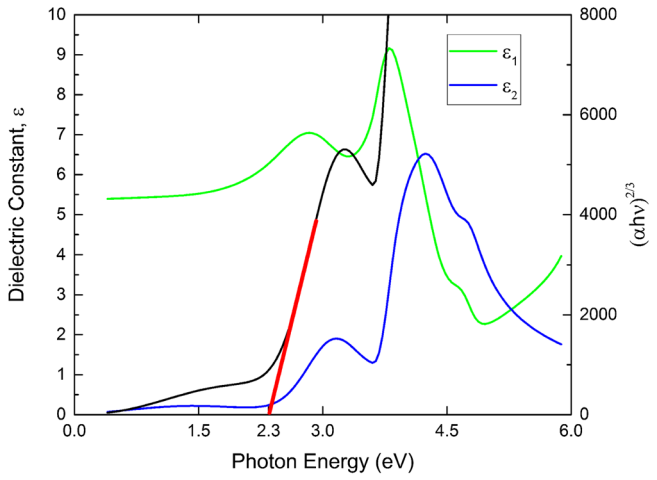

FIG. 2. Spectroscopic ellipsometry measurements of dielectric constants for a 12 nm LFO film on STO(001) (left axis) and determination of a direct forbidden band gap [black (red), right axis].

absorption coefficient, and $h\nu$ is the photon energy. Using the same approach (see Fig. 2), we find an identical band gap of 2.3 eV.

Based on our measurements of the VBO and the LFO band gap, along with the known STO indirect gap of 3.25 eV [21], we can construct energy diagrams for the LFO/n-STO heterostructure as a function of thickness. These are shown in Fig. 3, along with XPS valence band measurements for each sample. The points at −10 u.c. in Figs. 3(b)–3(d) represent the bulk and were calculated assuming an effective density of states at the conduction band edge for the distribution of electrons in Nb:STO. The LFO bands were determined based on the measured VBO and built-in potential gradients determined in Fig. 1, with

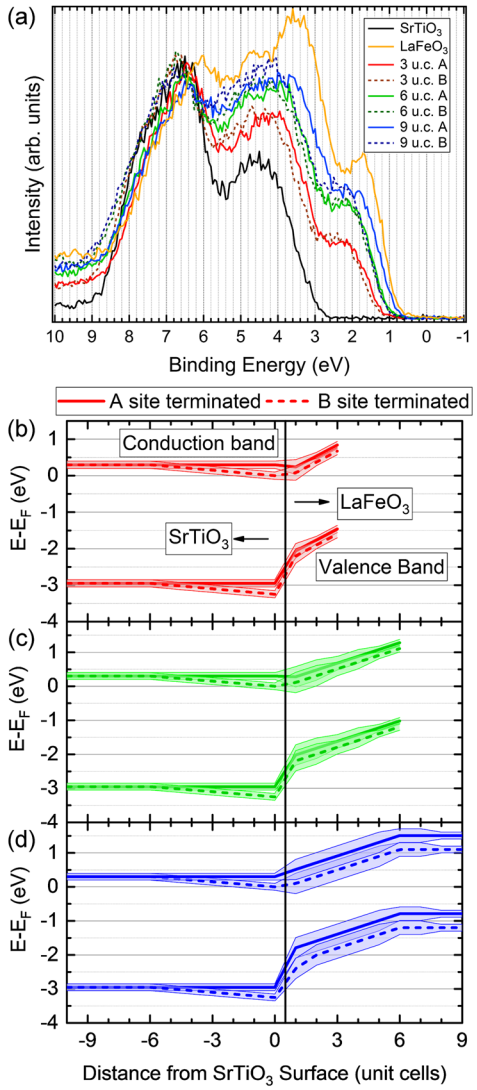

FIG. 3. (a) Valence band XPS spectra for bulk STO(001), a thick film of LFO(001), and all LFO/STO(001) heterojunctions (a). VBM (solid squares) and CBM (open squares) values taken from core-level binding energies for (b) 3, (c) 6, and (d) 9 u.c. LFO/n-STO. The values at 10 u.c. are representative of bulk STO and were calculated as described in the text.

the CBO determined using the LFO gap determined from ellipsometry [15]. The valence band maxima for the various LFO films extracted from the spectra shown in Fig. 3(a) are in excellent agreement with the values extracted from the energy diagrams shown in Figs. 3(b)–3(d).

Others have concluded that LFO is degenerately p type and that the interfacial conduction band offset (CBO) is ~1 eV [19]. However, we find that the LFO and STO conduction band minima are nearly degenerate at the interface for all thicknesses investigated. This result indicates that LFO is n type at the interface, with the possibility of some Fe^{2+} character due to carrier leakage from the n-STO. This finding is in agreement with other reports, which have shown that electron transfer occurs at the $LaTiO_3$/LFO interface, resulting in Fe^{2+} [22], and that Fe^{2+} is present in codoped $La_{2x}Sr_{1-2x}Fe_xTi_{1-x}O_3$ in which two La donors are present for every Fe acceptor [23]. After 6–9 unit cells, however, the conduction band levels off at higher energy, and E_F is approximately midgap in the LFO, making it an intrinsic semiconductor. This can be understood when one considers the instability of both holes from Fe^{4+} in (La, Sr)FeO_3 [6] and electrons from Fe^{2+} in Fe_3O_4 [24] in ambient conditions, indicating the high stability of Fe^{3+}.

The energy differences between STO VBM values for interfaces prepared from A- and B-terminated STO are consistent with the presence of a fixed charge of opposite sign. The VBM is closer to the Fermi level by 0.2–0.3 eV when the interface structure is nominally $(SrO)^0$-$(FeO_2)^{1-}$ than it is for the $(TiO_2)^0$-$(LaO)^{1+}$ interface structure. We say "nominal" because cation mixing occurs to some extent, resulting in modified interface charges. The difference in STO valence band energy between the two heterojunctions reveals that there is a difference in the magnitude of the potential gradient in the STO for the two heterostructures. The energy diagrams we present in Figs. 3(b)–3(d) reveal that the potential on the STO side of the $(TiO_2)^0$-$(LaO)^{1+}$ interface is nearly constant, while there is upward band bending on the order of 0.2–0.3 eV for the $(SrO)^0$-$(FeO_2)^{1-}$ case. The latter should promote hole drift from STO towards the LFO film. This result anecdotally supports the observations of K. Nakamura *et al.* [10], who rationalized variations in photocatalytic response by assuming downward band bending in the STO near the $(TiO_2)^0$-$(LaO)^{1+}$ interface, which, our data do not support. Qualitatively similar behavior might be observed if, instead, there is upward band bending that promotes hole drift towards the surface near the $(SrO)^0$-$(FeO_2)^{1-}$ interface and a flat-band condition at the $(TiO_2)^0$-$(LaO)^{1+}$ interface. In general, however, the band alignments that we observe are not expected to produce the dramatic differences in the photoresponse reported in Refs. [9,10]. Our results do not support the hypothesis of polarization in LFO pointing in opposite directions, and we suggest that other as yet undetermined mechanisms may be operative.

In summary, we synthesized a series of epitaxial $LaFeO_3$ films on n-doped $SrTiO_3$ with opposite surface terminations to study the effect of interface polarity on band alignment, potential gradients, and electronic reconstruction at the interface. We find that interface polarity has a negligible effect on the potential gradient within the films, in disagreement with previous reports of interface-controlled polarization in LFO. We do measure a slight difference in band bending on the STO side of the interface, presumably resulting from a screened fixed charge of opposite sign for the two interface polarities. However, it seems unlikely that this difference could account for the substantial differences in the photoresponse reported in the recent literature. We also have found the conduction band alignment between n-STO and LFO, showing that the CBO is $\sim$0 eV at the interface. These results provide important insights to understand the LFO/n-STO heterojunction for solar energy applications.

R. C. was supported by the Linus Pauling Distinguished Post-doctoral Fellowship at Pacific Northwest National Laboratory (PNNL LDRD PN13100/2581). S. C. was supported by the U.S. Department of Energy (DOE), Basic Energy Sciences (BES), Division of Materials Sciences and Engineering under Award No. 10122. A portion of this research was performed using EMSL, a national scientific user facility sponsored by the Department of Energy's Office of Biological and Environmental Research and located at Pacific Northwest National Laboratory.

[1] Z. Chen *et al.*, J. Mater. Res. **25**, 3 (2010).
[2] A. Duret and M. Grätzel, J. Phys. Chem. B **109**, 17184 (2005).
[3] S. Li, L. Jing, W. Fu, L. Yang, B. Xin, and H. Fu, Mater. Res. Bull. **42**, 203 (2007).
[4] K. M. Parida, K. H. Reddy, S. Martha, D. P. Das, and N. Biswal, Int. J. Hydrogen Energy **35**, 12161 (2010).
[5] M. D. Scafetta, A. M. Cordi, J. M. Rondinelli, and S. J. May, J. Phys. Condens. Matter **26**, 505502 (2014).
[6] S. Y. Smolin, M. D. Scafetta, A. K. Choquette, M. Y. Sfeir, J. B. Baxter, and S. J. May, Chem. Mater. **28**, 97 (2016).
[7] L. Li, P. A. Salvador, and G. S. Rohrer, Nanoscale **6**, 24 (2014).
[8] W. Ji, K. Yao, Y.-F. Lim, Y. C. Liang, and A. Suwardi, Appl. Phys. Lett. **103**, 062901 (2013).
[9] M. Nakamura, F. Kagawa, T. Tanigaki, H. S. Park, T. Matsuda, D. Shindo, Y. Tokura, and M. Kawasaki, Phys. Rev. Lett. **116**, 156801 (2016).
[10] K. Nakamura, H. Mashiko, K. Yoshimatsu, and A. Ohtomo, Appl. Phys. Lett. **108**, 211605 (2016).
[11] M. Kawasaki, K. Takahashi, T. Maeda, R. Tsuchiya, M. Shinohara, O. Ishiyama, T. Yonezawa, M. Yoshimoto, and H. Koinuma, Science **266**, 1540 (1994).
[12] H. J. Zhao, Y. Yang, W. Ren, A.-J. Mao, X. M. Chen, and L. Bellaiche, J. Phys. Condens. Matter **26**, 472201 (2014).
[13] R. B. Comes, P. Xu, B. Jalan, and S. A. Chambers, Appl. Phys. Lett. **107**, 131601 (2015).
[14] S. A. Chambers, T. C. Droubay, C. Capan, and G. Y. Sun, Surf. Sci. **606**, 554 (2012).
[15] See Supplemental Material at http://link.aps.org/supplemental/10.1103/PhysRevLett.117.226802 for RHEED images and discussion of XPS analysis, cation intermixing at the interface, and surface termination, which include Ref. [16].
[16] S. A. Chambers *et al.*, Surf. Sci. Rep. **65**, 317 (2010).
[17] R. B. Comes, S. R. Spurgeon, S. M. Heald, D. M. Kepaptsoglou, L. Jones, P. V. Ong, M. E. Bowden, Q. M. Ramasse, P. V. Sushko, and S. A. Chambers, Adv. Mater. Interfaces **3**, 201500779 (2016).
[18] S. A. Chambers, L. Qiao, T. C. Droubay, T. C. Kaspar, B. W. Arey, and P. V. Sushko, Phys. Rev. Lett. **107**, 206802 (2011).
[19] K. J. May, D. P. Fenning, T. Ming, W. T. Hong, D. Lee, K. A. Stoerzinger, M. D. Biegalski, A. M. Kolpak, and Y. Shao-Horn, J. Phys. Chem. Lett. **6**, 977 (2015).
[20] N. Nakagawa, H. Y. Hwang, and D. A. Muller, Nat. Mater. **5**, 204 (2006).
[21] S. A. Chambers, T. Droubay, T. C. Kaspar, and M. Gutowski, J. Vac. Sci. Technol. B **22**, 2205 (2004).
[22] J. E. Kleibeuker, Z. Zhong, H. Nishikawa, J. Gabel, A. Müller, F. Pfaff, M. Sing, K. Held, R. Claessen, G. Koster, and G. Rijnders, Phys. Rev. Lett. **113**, 237402 (2014).
[23] R. B. Comes, T. C. Kaspar, S. M. Heald, M. E. Bowden, and S. A. Chambers, J. Phys. Condens. Matter **28**, 035901 (2016).
[24] Ö. Özdemir, D. J. Dunlop, and B. M. Moskowitz, Geophys. Res. Lett. **20**, 1671 (1993).